ACS Chemical Neuroscience

pubs.acs.org/chemneuro Research Article

Identifying Neural Signatures of Dopamine Signaling with Machine Learning

Siamak K. Sorooshyari, Nicholas Ouassil, Sarah J. Yang, and Markita P. Landry*

Cite This: https://doi.org/10.1021/acschemneuro.3c00001 Read Online

ACCESS | Metrics & More | Article Recommendations | Supporting Information

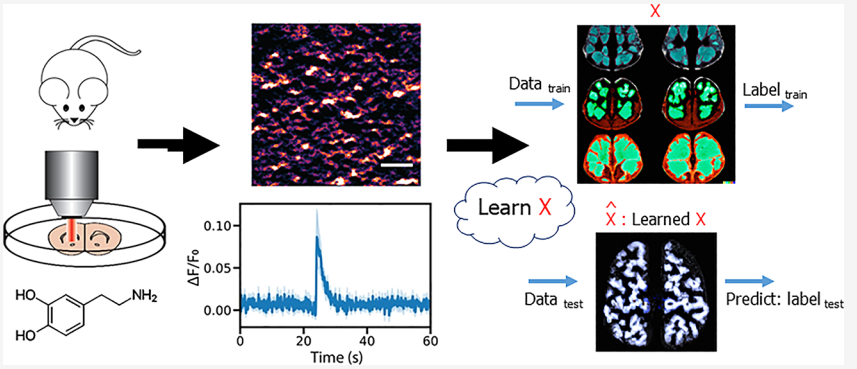

ABSTRACT: The emergence of new tools to image neurotransmitters, neuromodulators, and neuropeptides has transformed our understanding of the role of neurochemistry in brain development and cognition, yet analysis of this new dimension of neurobiological information remains challenging. Here, we image dopamine modulation in striatal brain tissue slices with near-infrared catecholamine nanosensors (nIRCat) and implement machine learning to determine which features of dopamine modulation are unique to changes in stimulation strength, and to different neuroanatomical regions. We trained a support vector machine and a random forest classifier to decide whether the recordings were made from the dorsolateral striatum (DLS) versus the dorsomedial striatum (DMS) and find that machine learning is able to accurately distinguish dopamine release that occurs in DLS from that occurring in DMS in a manner unachievable with canonical statistical analysis. Furthermore, our analysis determines that dopamine modulatory signals including the number of unique dopamine release sites and peak dopamine released per stimulation event are most predictive of neuroanatomy. This is in light of integrated neuromodulator amount being the conventional metric used to monitor neuromodulation in animal studies. Lastly, our study finds that machine learning discrimination of different stimulation strengths or neuroanatomical regions is only possible in adult animals, suggesting a high degree of variability in dopamine modulatory kinetics during animal development. Our study highlights that machine learning could become a broadly utilized tool to differentiate between neuroanatomical regions or between neurotypical and disease states, with features not detectable by conventional statistical analysis.

KEYWORDS: *dopamine, machine learning, nanosensors, striatum*

INTRODUCTION

Recent advances in the ability to image neuromodulators from single neurons,[1] in acute brain slices[2] and in vivo,[3,4] have enabled insights into the role of neurochemical communication in the neurotypical and diseased brain. The newly accessible neurochemical signals could greatly advance neuroimaging by providing an additional dimension of information regarding the role of neuromodulation in regulating brain circuits and the central role of neuromodulators in psychiatric and neurodegenerative disease. Specifically, several dopamine probes have been developed in the past few years that have achieved imaging of dopamine at spatiotemporal scales commensurate with endogenous neurochemical signaling. A class of genetically encoded probes have enabled cell-specific expression of protein-based reporters that fluoresce when dopamine is bound.[3,4] Additionally, synthetic dopamine nanosensors have recently been developed based on the adsorption of $(GT)_6$ single-stranded DNA oligonucleotides on the surface of single-walled carbon nanotubes (SWNT), to generate a $(GT)_6$-SWNT nanosensor that is responsive to dopamine with fluorescence modulation exceeding 2500%.[24] These synthetic nanosensors

Received: January 1, 2023
Accepted: May 22, 2023

have recently been used to image dopamine modulation in acute brain slices,[2] to elucidate dopamine modulatory deficits in Huntington's Disease[9] and have achieved single dopamine release site resolution to directly image somatodendritic dopamine signaling in primary neurons[1] and dopamine release at axonal varicosities.[25] As these neuroimaging tools are implemented more broadly, it becomes imperative to interpret the biological underpinnings of the signals and understand the features of importance of this previously 'invisible' dimension of neurobiology. Recent studies,[20−23] have used machine learning to analyze dopamine electrochemical traces, enabling differentiation between catecholamines with similar redox potentials and dopamine enantiomers that raw analysis of traces would not enable. However, to our knowledge, dopamine imaging datasets with high-dimensional dopamine probes have yet to be achieved. Herein, we implement several machine learning approaches to identify and evaluate what features extracted from dopamine imaging studies distinguish neurobiological features of importance, and which machine learning approaches enable the analyses.

Male B6CBA-Tg(HDexon1)62Gpb/3J mice (R6/2 mice) were purchased from Jackson Labs and bred at 6 weeks with 10-week-old female C57BL/6 mice. Near-infrared catecholamine nanosensors (nIRCat) have enabled imaging of neuromodulator dopamine in brain tissue[2] and to study the role of its modulation in neurodegeneration.[9] nIRCat is a versatile synthetic optical tool for monitoring dopamine release and reuptake in acute slices and is compatible with a broad range of pharmacological agents used to target dopamine receptor activity. nIRCat provides high spatial (micron) and temporal (second) resolution videos of dopamine modulation in the brain extracellular space, with many features contributing to the signatures of dopamine release and reuptake through its volume transmission in the extracellular space. This enables time-resolved imaging of dopamine modulation at the level of individual synapses. In this study, we use nIRCat to image electrically-stimulated dopamine release within the dorsal striatum of acute brain slices generated from 4-, 8.5-, and 12-week-old, wildtype mice. It is important to note that the 4-week-old mice represent prepubescent young animals, while the 12-week-old mice have reached adulthood. Striatal tissue provides an ideal environment for measuring dopamine with nIRCats since this brain region is rich in dopaminergic projections from the substantia nigra and relatively little norepinephrine, i.e., there is a faction of norepinephrine in the striatum in comparison to the amount in the cortex.[26] Moreover, we assess whether machine learning can be implemented to identify if dopamine modulatory signals can distinguish striatal subregions, and which features of neurotransmitter modulation are most predictive to identify different brain regions. Specifically, we apply two conventional yet distinct machine learning techniques to analyze stimulated dopamine release imaged with nIRCat in the dorsolateral striatum (DLS) and the dorsomedial striatum (DMS). Stimulated dopamine release is achieved with a single pulse at either 0.1 or 0.3 mA stimulation strength. The two machine learning approaches we implemented are a support vector machine (SVM) and, separately, a random forest (RF) approach. We selected a SVM because of its capability to distinguish observations into separate classes based on the features that may share complex, nonlinear relationships with the different classes to which the observations belong. The SVM notion is based on finding a boundary in a space that separates the training data into distinct classes and then applying that same boundary or rule to the test data. We selected the RF approach because it is a relatively simple method that will allow interpretation of which variables from our dopamine imaging datasets enable the most accurate predictions. RF is an ensemble method, where multiple decision trees are formed on the same dataset. The individual decisions made from each decision tree are then combined to arrive at a consensus on the outcome that is output as the classification. The classification decision is output after the decision criteria for each split at a node of a tree are determined based on the training data in supervised fashion. The intricacy of RF that distinguishes it from its decision tree relatives is that RF decorrelates the decision trees by considering only a subset of features at each split in a constituent tree. This approach prevents the possibility of one or a small portion of the features dominating the decisions.

In our experimental workflow, we stimulated nIRCat-labeled acute striatal slices with a single 0.1 or 0.3 mA pulse and imaged dopamine release in the DLS and DMS striatal regions of mouse brain tissue. Our hypothesis is that any differences in dopamine release in DLS versus DMS could be elucidated from our nIRCat data features, and that machine learning approaches can unearth whether dopamine imaging is alone sufficient to distinguish the DLS from DMS. Recent study has shown differences in signaling, specifically differences in peak dopamine concentration between dorsal and ventral subregions of the striatum in mice. In ref 7, Calipari et al. found that DLS produces a roughly 4× higher concentration of stimulated dopamine release than the Nucleus Accumbens core when measured in acute brain slices with fast-scan cyclic voltammetry.[7] However, somewhat contradictory results have been reported using R6/2 mice, in which no significant differences in maximum dopamine release were observed across striatal subregions.[8] Known differences in dopamine transporter levels across the dorsal striatum indicate that peak concentration may not fully capture signaling disparities in the basal ganglia, and that regional differences in autoreceptor expression, differences in axonal architectures, or differences in projection density may contribute to signaling kinetics.[12−14] We, therefore, sought to study which dopamine signaling features contribute to regional differences in modulatory kinetics and assess whether machine learning approaches may provide a user-removed means for identifying subtle changes between brain regions in a manner that considers more than absolute dopamine release concentrations. We further hypothesize that machine learning can identify which features of dopamine modulation enable this differentiation. We anticipate that the identification of features of stimulated dopamine release to be important for differentiating neuroanatomy and that the role of machine learning for this goal will provide important insights for the interpretation of neuromodulator imaging experiments.

RESULTS AND DISCUSSION

Collected Data. Male B6CBA-Tg(HDexon1)62Gpb/3J mice (R6/2 mice) were purchased from Jackson Labs, which we bred at 6 weeks with 10-week-old female C57BL/6 mice. Mice were kept in temperature-controlled environments with three to five mice per cage on a 12 h light/dark cycle, with all animal procedures approved by the University of California, Berkeley Animal Care and Use Committee (ACUC). We synthesized our dopamine nIRCat nanosensor and used nIRCat to label acute live brain slices, as described previously in ref 10. Acute brain slices were then labeled with nIRCat through passive incubation in 5 mL of ACSF containing nIRCat

https://doi.org/10.1021/acschemneuro.3c00001
ACS Chem. Neurosci. XXXX, XXX, XXX−XXX

nanosensor at a concentration of 2 mg/L for 15 min, rinsed, and placed in a recording chamber to equilibrate during which a tungsten bipolar stimulation electrode was positioned in the striatal region of interest. We applied a single electrical stimulation pulse of 0.1 or 0.3 mA after collecting 200 frames of baseline nIRCat fluorescence from two brain regions: DLS and DMS. To reduce bias, all stimulation videos were collected in triplicate and we alternated stimulation strengths. Next, nIRCat-labeled brain tissue slices were processed to quantify their response to stimulated dopamine release. Raw image stack files were processed using a custom-built, publicly available MATLAB program with the image processing protocol described in depth elsewhere.[10] These processed data form the inputs of our machine learning algorithms, summarized in Table 1, and are calculated as follows: regions of dopamine release in acute slice tissue are identified by large changes in nIRCat $\Delta F/F$ response. Dopamine hotspots were programmatically identified by creating a grid of 2 μm squares across the field of view to reduce bias and expedite image stack processing time. The relationship $(F - F_0)/F_0$ was used to calculate the change in fluorescence, $\Delta F/F$, of each grid square. Herein, F_0 represents the average fluorescence of the grid square over the first 30 frames of the image stack and F is the fluorescence intensity of the grid square as it changes over the 600 collected frames. The program identifies dopamine hotspots as regions of interest (ROI) with statistically significant dopamine release activity if these grid squares exhibit nIRCat fluorescence behavior that is at least 3 standard deviations above the baseline fluorescence activity, F_0, at the time of slice stimulation (200 frames). In this manner, we identified dopamine release hotspots for each stimulation image stack for nIRCat-labeled brain slices. The peak fluorescence, $\Delta F/F$, of each dopamine hotspot in the image stack was averaged to generate the average image stack peak $\Delta F/F$. The number of active dopamine release sites per stimulation event per brain slice were then identified and averaged to output the average slice hotspot number. Mean values for dopamine release and reuptake curves were calculated from averaging traces from each slice, including three stimulations per slice and 1 slice per mouse. These outputs were subsequently used to assess the feasibility of machine learning to distinguish differences in features, such as peak $\Delta F/F$ or dopamine hotspot number, across stimulation strengths and across brain regions. Table 2 lists the experimental conditions and number of independent stimulations used for each experimental condition, and Table 1 lists the collected and analyzed data from nIRCat-labeled brain slices subjected to single-pulse stimulation for dopamine release. It is worth noting that while our analysis is based on temporal traces generated from stimulated tissue videos, the traces represent dopamine released from individual release sites measuring on average ~2 μM in size, thus preserving the spatial advantage of dopamine imaging over electrochemical measurements.

Table 1. Features Computed from Traces To Be Used in the Machine Learning Analysis[a]

Feature	Description
E[dF]	mean of dopamine dF trace
Var[dF]	variance of dopamine dF trace
med[dF]	median of dopamine dF trace
min[dF]	minimum dopamine dF trace
max[dF]	maximum dopamine dF value in recording
ROI count	number of dopamine release sites (ROIs) in the brain slice field of view
AUC of dF	area under the dopamine dF curve
decay of dF	dopamine reuptake kinetics calculated by an exponential decay fit to the dopamine dF trace
ND-low	number of times dF was lower than the -2σ level
ND-high	number of times dF exceeded the 2σ level

[a]Features were calculated for each recording and used as the inputs to the algorithms. The first 8 features (red) are deemed as statistical features whereas the last 2 features (blue) are referred to as paroxysmal features. In several of the ML analyses, all 10 features were simultaneously used. In most dopamine imaging literature only one value, the mean dopamine signal as a function of time, is considered for analysis.

Table 2. Distribution of Brain Regions and Stimulation Strengths That Were Recorded in Mouse Brain Slices

time point	animals	slices	stimulation strength (mA)	DLS (N stimulations)	DMS (N stimulations)
4 weeks	7	16	0.1	27	16
			0.3	25	16
8.5 weeks	9	20	0.1	32	22
			0.3	18	18
12 weeks	5	13	0.1	22	18
			0.3	22	15

Computed Features. Acute coronal brain slices were generated to contain the dorsal striatum and labeled with nIRCat nanosensor (Figure 1A), as described previously,[2] to image stimulated dopamine release, as described above and schematically depicted in Figure 1B,C. Time series traces were used to generate the data features listed in Table 1, and prior to this study it was unknown which of these features would be most informative for distinguishing DLS from DMS or for analysis of neurochemical modulation data as a whole (Figure 1D). Table 1 summarizes the features that were analyzed from each brain slice labeled with nIRCat and following electrical stimulation. This contrasts with the usual practice of considering the mean dopamine value as a function of time for dopamine imaging in neurobiological datasets. We also provide a representative intensity trace annotated to highlight the features used in the present study (Figure 1D). The number of active putative dopamine release sites, termed ROIs, are programmatically identified, as described previously[2] and represent dopamine release sites. Each individual ROI, in turn, includes a series of features associated with dopamine release and reuptake from a single dopamine release site, which includes maximum change in fluorescence (max dF), area under the dopamine response curve (AUC), and dopamine signal decay (τ). Max dF is proportional to the maximum concentration of dopamine measured by nIRCat at that release site. AUC represents the integrated area under the ROI fluorescence curve following stimulated release and is a relative measurement of the total amount of dopamine released by a site. Signal decay represents the reuptake kinetics of dopamine, a signal that is dependent on the expression and activity of dopamine transporters in brain tissue within the ROI. Each of these features are computed over the duration of each recording to attain the mean, variance, median, minimum, and maximum values. The last two features in Table 1 reflect the number of "deviations" for a recording, termed paroxysmal features. Specifically, the signal from each stimulated brain slice was Z-scored and a deviation-high was declared when the recording exceeded a value of 2 standard deviations from the

https://doi.org/10.1021/acschemneuro.3c00001
ACS Chem. Neurosci. XXXX, XXX, XXX−XXX

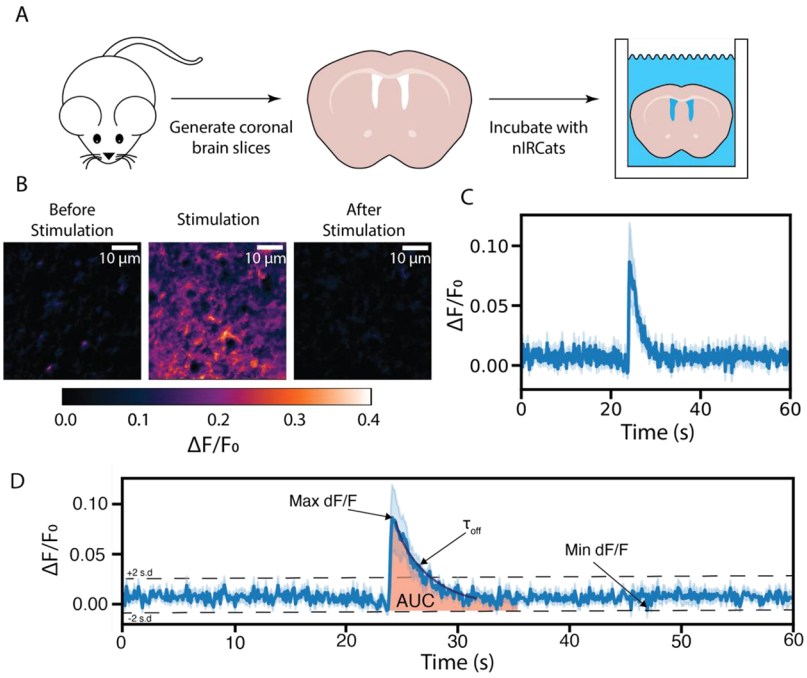

Figure 1. Feature extraction procedure of using nIRCat to image electrically-stimulated dopamine release in mouse brain slices. (A) Cartoon depiction of generation of nIRCat-labeled brain slices. (B) Representative images of stimulated dopamine release in acute striatal slices. (C) Processed dopamine trace depicting neurotransmitter release after electrical stimulation from a single dopamine release site. (D) A single dopamine trace annotated with the mined features.

mean, similarly a deviation-low was declared when the recording fell 2 standard deviations below the mean. The number of low and high deviations in a recording are referred to as ND-low (ND: number of deviations) and ND-high, respectively. In training machine learning algorithms and making ensuing predictions, we consider the combination of all 10 features from Table 1, as the combined feature set.

Machine Learning Algorithm Development. The SVM and RF algorithms were trained on the features in Table 1, first to assess whether these algorithms could differentiate between dopamine released from nIRCat-labeled slices stimulated at either 0.1 or 0.3 mA stimulation strengths. Prior literature using nIRCat-labeled brain slices shows that different stimulation strengths generate proportionately different levels of dopamine release, with higher stimulation amplitudes generating a higher max dF/F and AUC.[2] Therefore, we trained our algorithms on data for which the dopamine release differences are known. The SVM algorithm used a linear kernel with a binary classifier. With the kernel denoting a function that reflects the similarity among observations—the use of a linear kernel leads to the boundary between the classifier's decisions being a linear function of the considered features. The choice of a binary classifier was made because in each prediction, we are considering two alternatives, i.e., distinguishing between DLS/DMS regions or distinguishing between 0.1/0.3 mA stimulation strengths. For the predictions that are made in our analysis, the linear kernel was selected for its simplicity and the absence of detailed a priori knowledge regarding which of the dopamine features would be most important in distinguishing between stimulation strengths and eventually between brain regions from which dopamine originates. We did not consider the RF algorithm with paroxysmal features as there were too few features (i.e., $p = 2$) to consider this as worthwhile analysis. We next evaluated the predictive capability with the SVM and RF algorithms via a leave-one-out analysis with Monte-Carlo sampling of all animals and brain slices. The Monte-Carlo analysis consists of the data being repeatedly divided into a training and test set with the test data consisting of a single observation, while the remaining data was evenly partitioned into two groups and used to train the machine. The computational pipeline is depicted in Figure 2 and was used to make predictions from the considered data.

Machine Learning Can Distinguish Dopamine Release at Different Stimulation Strengths. Stimulation of nIRCat-labeled brain slices shows higher dopamine release as a function of stimulation strength, as expected and previously demonstrated.[2] Therefore, to validate the ability of our machine learning algorithm to distinguish between dopamine modulatory behavior with a known dependence on experimental condition, we first assessed whether our algorithms could distinguish between nIRCat-labeled brain slices stimulated with 0.1 or 0.3 mA stimulation strengths. To avoid the confounding effect of brain region on this analysis, we compared 0.1 mA versus 0.3 mA stimulation in DLS separately from DMS.

The SVM and RF algorithms were implemented with the different groups of features listed in Table 1. Running SVM with all 10 features is denoted via SVM (10), while using only the 8 statistical and 2 paroxysmal features is denoted by SVM (8) and SVM (2), respectively. The same notation is used with the RF algorithm—i.e., RF (10) represents implementing RF with all 10 features. The pipeline in Figure 2 was followed to attain an AR for each of the stimulation strengths. Our results indicate that an accurate discernment of the stimulation strength in the DLS and DMS is not possible from brain slices generated from 4- and 8.5-week-old mice with SVM or RF algorithms, although SVM performed slightly better in the DLS than in the DMS at 4 weeks. At 4 weeks, the aggregate accuracy ("aggregate" denotes averaging the 0.1 and 0.3 mA results to provide a holistic account) in the DMS does not exceed chance, while the best discernibility occurs from data taken in the DLS with the SVM algorithm and is 0.557 (Figure 3A). At 8.5 weeks, nIRCat

https://doi.org/10.1021/acschemneuro.3c00001
ACS Chem. Neurosci. XXXX, XXX, XXX−XXX

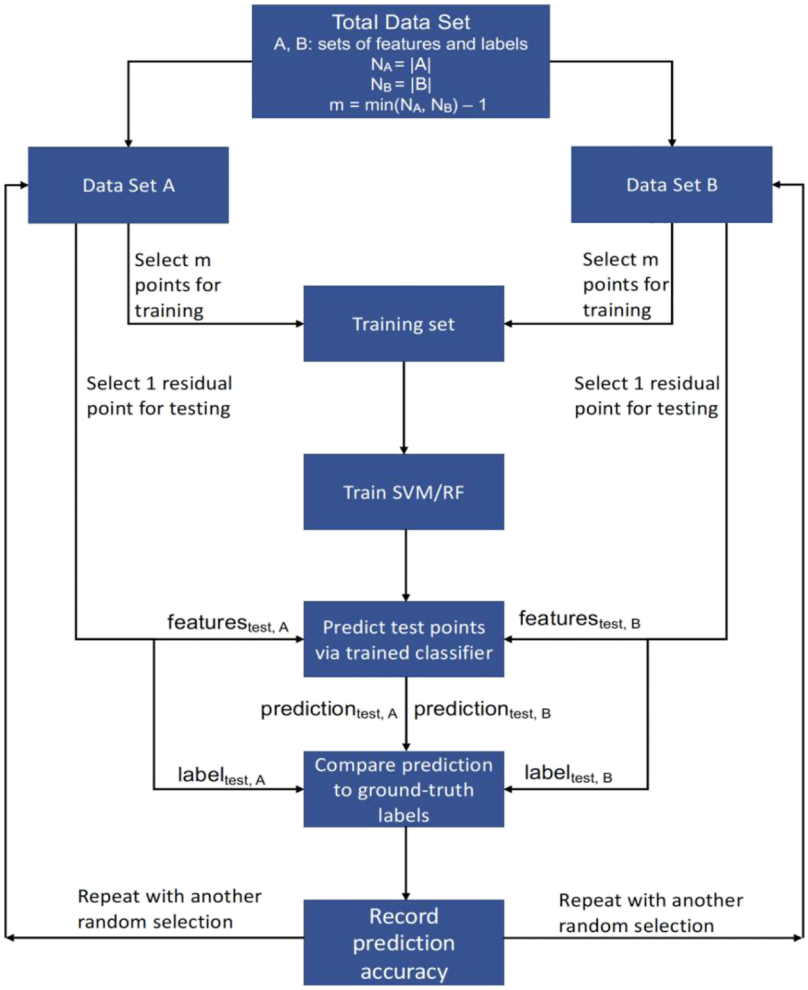

Figure 2. Machine learning workflow to predict the electrical stimulation strength applied to brain slices or the brain regions of dopamine release. The sets A and B may correspond to the groups of brain slices stimulated at 0.1 or 0.3 mA—alternatively, the sets may correspond to the groups of brain slices stimulated in the DMS or DLS. The notation |.| refers to the number of elements in the set (i.e., cardinality). The above sequence is repeated 1000 times to arrive at a classification accuracy rate (AR). Each iteration encompasses a SVM or RF being trained on features from training data prior to the machine being presented with one left-out data point from each of the two groups. The AR is attained by computing the fraction of times the labels of the left-out samples from set A and B were correctly predicted as being equal to their ground-truth values.

features provide a better indication for whether a 0.1 or 0.3 mA stimulation amplitude was used in the DMS region with the best AR being 0.649 for the RF (8) algorithm. Here, the aggregate accuracy in the DLS barely exceeds chance (Figure 3B). However, as mice age to 12 weeks, the distinguishability generally increases when using the SVM or RF algorithms in both the DLS and the DMS brain regions. At 12 weeks, the aggregate accuracy in both DLS and DMS consistently exceeds chance for both algorithms, with the best discernability occurring from data taken in the DLS with the RF algorithm at an AR of 0.832 (Figure 3C). For the ML analysis, we evaluate statistical significance by considering the aggregate predictive ARs that exceed 0.65, which is approximately one sigma greater than the chance value of 0.5 (binary classification). It is interesting that the prediction accuracy of our machine learning algorithms consistently increases as a function of animal age, going from chance at 4 weeks to maximum ARs of 0.649 (RF (8)) at 8.5 weeks and 0.832 (RF (8)) at 12 weeks. Importantly, we note that the 12-week-old animal cohort exclusively exhibits prediction accuracies exceeding 0.65 (Figure 3C). These results suggest that dopamine signaling variability in young animals is larger than adult animals, and that this variability precludes machine learning based discrimination of stimulation strength. Biologically, a 4-week-old mouse corresponds to a prepubescent young animal, with the 8.5-week timepoint representing mice that have shifted into sexual maturity, and 12-week-old mice well into adulthood. Our results confirm that dopamine dynamics are still developing across our timepoints, with much more variability in the kinetics and features of dopamine release in young animals that confounds machine learning algorithms and prevents distinguishing stimulation strengths in 4 (and to a lesser extent 8.5) week-old animals. Interestingly, by the time animals age into adulthood (12 weeks). It is possible that dopamine release and reuptake features have stabilized and enable us to clearly distinguish between stimulation strengths. This indeed represents the adult age group of prior work showing increasing dopamine release as a function of stimulation strength.[2] These results are important because they suggest that dopamine measurements taken in prepubescent animals undergoing development may introduce a high degree of biological variability and may prevent experimentation using dopamine signaling outputs as the sole form of measurement, particularly when the predicted biological effect size is small or moderate. Conversely, dopamine imaging

https://doi.org/10.1021/acschemneuro.3c00001
ACS Chem. Neurosci. XXXX, XXX, XXX−XXX

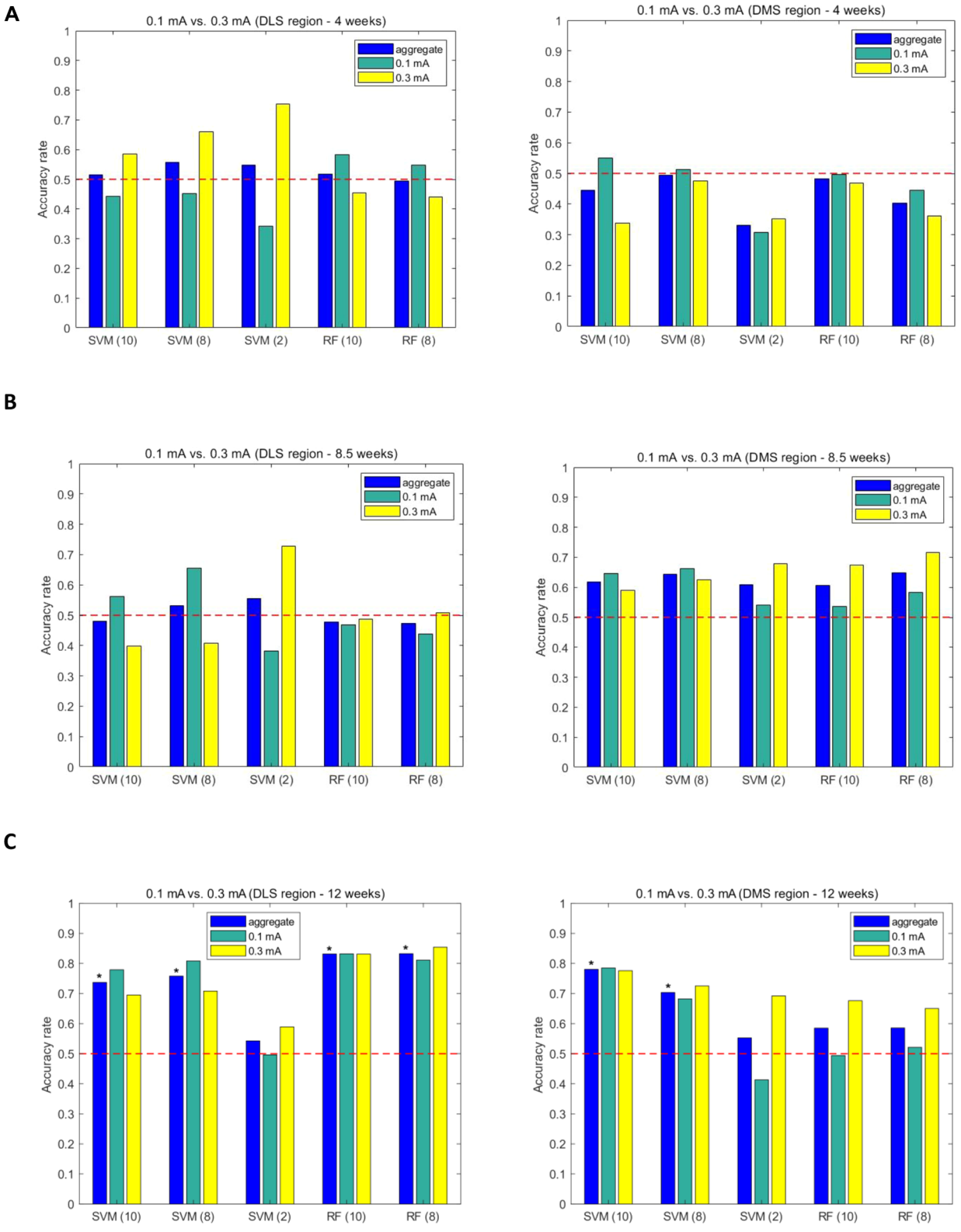

Figure 3. Predictive accuracy in distinguishing between 0.1 and 0.3 mA stimulation strengths of the DLS and DMS. Different time points were considered in the ages of the mice—subfigures (A), (B), and (C) correspond to results for the data collected from animals of 4, 8.5, and 12 weeks of age, respectively. The asterisk denotes significance in the aggregate predictive capability exceeding the 0.65 AR, which is approximately one sigma greater than the chance value of 0.5 (binary classification).

measurements taken from adult animals exhibit less biological variability, enabling our machine learning algorithms to clearly distinguish between the stimulation amplitudes used, as expected.

Machine Learning Algorithm Implemented To Explore Dopamine Modulatory Differences between the DLS and DMS Brain Regions. Having confirmed that our SVM and RF algorithms are able to distinguish between brain

https://doi.org/10.1021/acschemneuro.3c00001
ACS Chem. Neurosci. XXXX, XXX, XXX−XXX

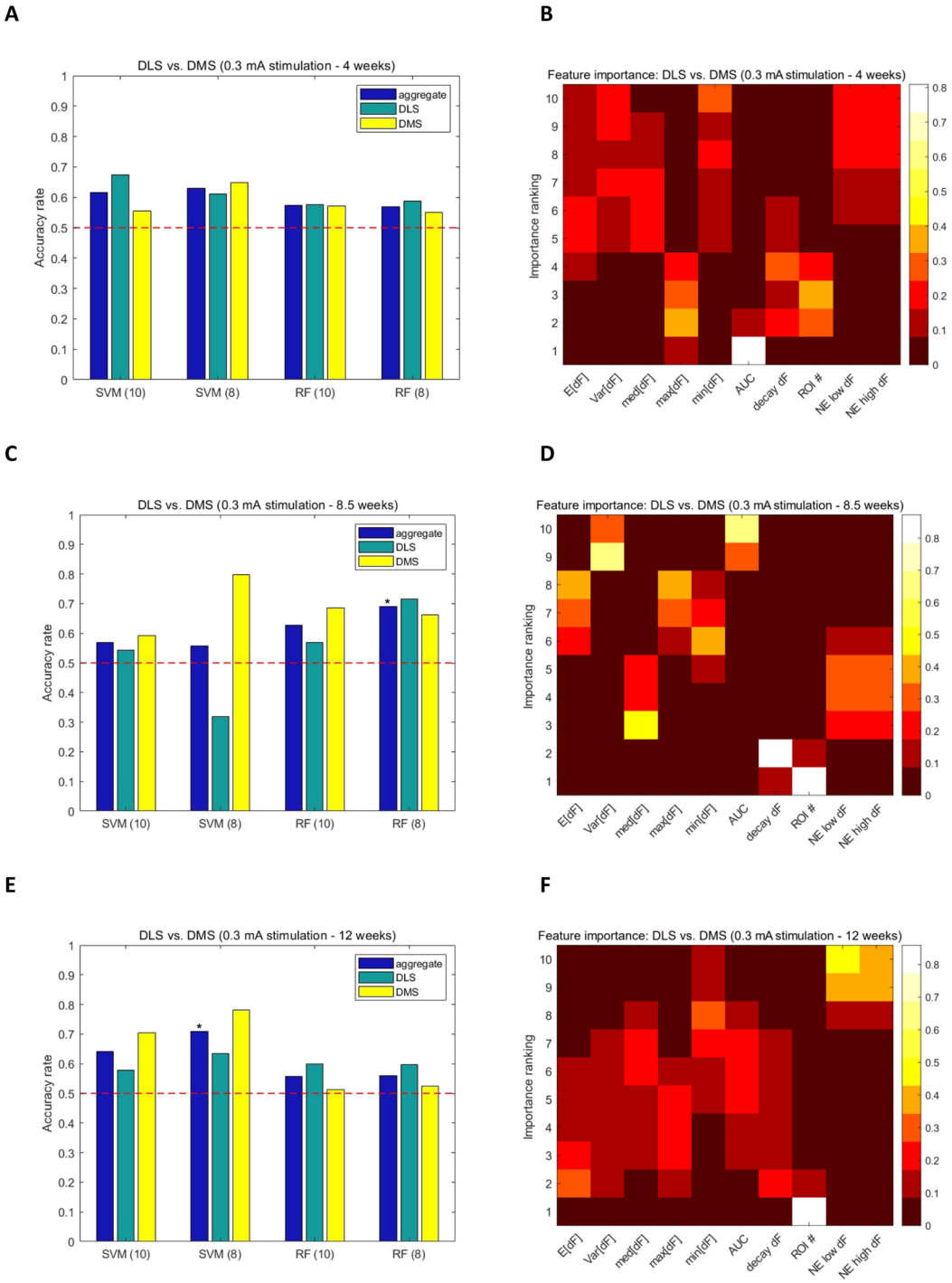

Figure 4. Predictive accuracy and feature importance rankings attained with the machine learning pipeline. Accuracy of predicting whether a recording was made from the DLS or DMS at a stimulation strength of 0.3 mA. The quantities in the parentheses indicate the number of features that were used to train the machine and form the test data in the machine learning analysis. The subfigures (A), (C), and (E) correspond to results for the data collected from animals of 4, 8.5, and 12 weeks of age, respectively. The asterisk denotes the significance in the aggregate predictive capability exceeding the 0.65 accuracy rate, which is approximately one sigma greater than the chance value of 0.5 (binary classification). The corresponding heatmaps (B), (D), and (F) illustrate a ranking of each feature's importance in contributing to the RF classification decision when 10 features (Table 1) were used.

tissue slices stimulated at 0.1 or 0.3 mA in adult mice, we next sought to determine whether machine learning could be used to distinguish DLS or DMS striatal brain regions based only on the dopamine release and reuptake features from each region. To this end, we implemented the Monte-Carlo technique with 1000 iterations with the SVM and RF algorithms. To use a balanced training set for the predictive analysis, an equal number of DLS and DMS brain slices were used to train the machine prior to testing on one held-out DLS and DMS brain slice, which represent a recording that was not used as part of the training data. The AR in predicting whether a recording was made from the true striatal brain region was evaluated by counting the number of times that a correct classification was made for the held-out DLS and DMS samples across all iterations. The result

https://doi.org/10.1021/acschemneuro.3c00001
ACS Chem. Neurosci. XXXX, XXX, XXX−XXX

is normalized by the number of iterations, 1000, used as part of the pipeline, and an aggregate AR was computed by averaging the AR of held-out data from the DLS with that attained with held-out data from the DMS. The choice of 1000 iterations was deemed large enough to sufficiently cover the number of combinations (i.e., Monte-Carlo sampling) of leave-one-out scenarios. The differences in the results seen with a higher number of iterations were negligible. We consider the predictive capability of our algorithm as being acceptable if the two constituent ARs exceed the chance value of 0.5. Chance is a sufficient cutoff value since expert experimenters were unable to identify any of the tested classification problems better than the chance rate. The steps for the analysis and the prediction on test data are depicted in Figure 2, and the machine learning pipeline is the same as we used to assess whether the stimulation strength—i.e., 0.1 or 0.3 mA—can be determined from the dopamine modulatory signals.

It is often beneficial to be cognizant of the features that are the most important in making a classification, whether it be to distinguish stimulation strength or brain region. The RF machine learning algorithm is a tree-based method that readily provides an account of the features that are the most important in arriving at its decisions. Biologically, it is possible that certain features may be more important in distinguishing stimulation strengths or brain regions—e.g., to distinguish between stimulation strengths, a higher stimulation amplitude may evidently increase the max dF/F (more dopamine) without affecting the decay of dF (the rate at which dopamine is cleared from tissue). Conversely, differences in dopamine transporter expression in DLS versus DMS may affect dopamine clearance rates from tissue without affecting dopamine release features. For the development of our RF algorithm, we therefore utilized a node purity metric to evaluate which of the stimulated dopamine features are the most important to the RF technique's decisions. The node purity metric is equated to the total variance computed across the classes, with lower variance levels associated to a feature implying that in the trees' arriving at a decision, a decision based on that feature contained a high percentage of data from one class (i.e., 0.1 mA vs 0.3 mA or DLS vs DMS). Thus, the node purity metric provides a quantitative measure of the features' importance in the RF classification decision. Unlike the RF algorithm that accounts for the relative contribution of each feature in arriving at its decision, the SVM algorithm does not. For SVM, the solution is a vector that determines a hyperplane setting the boundary between the decision regions. The vector for SVM is the solution of a quadratic optimization problem, and the variable selection is typically applied by penalizing a norm on the optimization vector to suppress unimportant features from appearing in the solution. An alternative brute-force means of performing feature selection for SVM involves iteratively removing features or groups of features and evaluating the accuracy of the procedure on portions of the data set.

Differentiating Dopamine Release from DLS versus DMS with nIRCat Recordings. We next used the machine learning pipeline developed to differentiate dopamine dynamics to study nIRCat recordings from the DLS and DMS of acute brain slices collected from 4-, 8.5-, and 12-week-old mice, as depicted in Figure 2. For this approach, we used data only from 0.3 mA stimulations, as they provided clearer nIRCat signals than the lower 0.1 mA stimulation amplitudes. SVM and RF approaches were used to process stimulated dopamine imaging videos on datasets segregated by animal age. The results, as shown in Figure 4, indicate that at 4 weeks of age, SVM provided better ability to distinguish whether dopamine was imaged from the DLS or DMS of a brain slice: an SVM operating on the 8 statistical features, as listed in Table 1 provided the best performance via an AR of 0.615. RF also provided above-chance predictive capability, with an AR of 0.573 and 0.569 for the combined and statistical features, respectively, but inferior to that attained with the SVM for the same considered feature groups (Figure 4A). Conversely, at 8.5 weeks, the best differentiation in whether dopamine was released from the DLS or DMS is achieved with the RF algorithm. The aggregate ARs with RF exceed 0.6, with an AR of 0.69 noted when using all 8 statistical features. At 8.5 weeks, the SVM performance with the combined features is only marginally above chance with an aggregate accuracy rate of 0.568. For this latter scenario, the machine trained on nIRCat recordings classifies the majority of dopamine release events as having arisen from the DMS (Figure 4C). Thus, a rather high accuracy rate of 0.798 is noted in differentiating DMS recordings, but poor aggregate accuracy is apparent via the classification of the majority of DLS dopamine releases said to have stemmed from the DMS. Explicitly, out of the 1000 iterations, 798 iterations were accurately classified as being via DMS stimulation, whereas only 318 iterations were accurately classified as having resulted from DLS stimulation. At 12 weeks, the SVM again yields superior predictive capability over RF with accuracy rates of 0.64 with the 10 (i.e., combined) features, and 0.708 with 8 statistical features (Figure 4E). At each of the three animal ages, the use of the paroxysmal features did not provide above-chance predictive accuracy of enabling differentiation of the signal as having originated from DLS or DMS. In general, higher accuracy rates are noted in Figure 4 when considering the statistical or combined features rather than paroxysmal features (not pictured). The better accuracies obtained with statistical or combined features highlights the importance of considering statistical rather than transient or paroxysmal aspects of the dopamine recordings for the purpose of identifying the striatal region from which those dopamine modulatory features originate. In summary, at the three considered animal ages, when providing a 0.3 mA stimulation pulse to elicit dopamine release, nIRCat dopamine images and their features provide a biomarker for differentiating whether the dopamine was released from the DLS or DMS region. Interestingly, the predictive capability in differentiating the brain region with 0.3 mA electrical stimulation increased as a function of animal age, similarly to our age-dependent ability to use machine learning algorithms to distinguish between stimulation strengths. Specifically, the best aggregate accuracy rate at 4 weeks was 0.629, while at 8.5 and 12 weeks, we noted accuracy rates of 0.69 and 0.708, respectively. These results support our prior findings and hypothesis that early in animal development there exists high variability in dopamine release and reuptake activity in a manner that equilibrates in adulthood.

Feature Importance for Differentiating DLS from DMS with Dopamine Modulatory Signatures. We have confirmed that stimulated dopamine release imaging in acute slices provides machine learning algorithms, such as SVM and RF, the ability to distinguish between stimulation strength (0.1 mA vs 0.3 mA) and brain region (DLS vs DMS). Interestingly, we also find that our predictive capabilities are directly proportional to animal age, supporting the hypothesis that dopamine signaling dynamics are more variable early in development and stabilize in adulthood. We next determined which features of our dopamine recordings are most important for the predictions that were

https://doi.org/10.1021/acschemneuro.3c00001
ACS Chem. Neurosci. XXXX, XXX, XXX−XXX

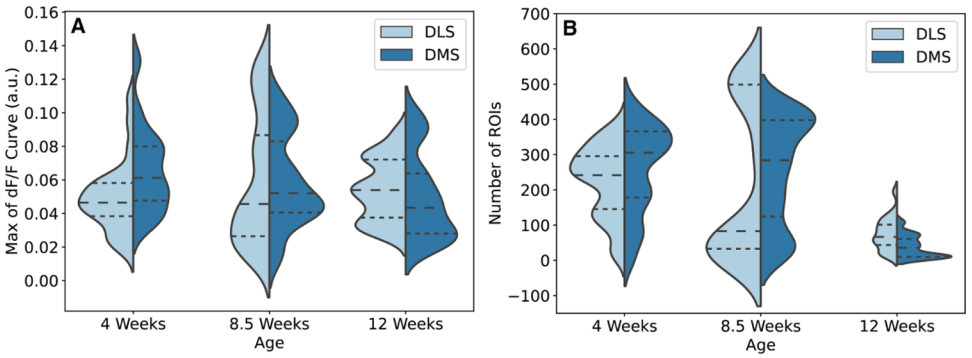

Figure 5. Univariate distribution of several features deemed important for distinguishing DLS from DMS brain regions. Violin plots of max[dF] (A) and ROI number (B) across age groups for DLS (light blue) versus DMS (dark blue) brain regions. The dashed lines indicate the 25th, 50th, and 75th percentiles of the distribution.

made by the machine learning analyses. With RF, the node purity measure was used to determine the feature importance. The heatmaps in Figure 4B,D,F provide an account of the frequency at which each of the 10 considered dopamine recording features were ranked in their importance for arriving at a prediction. For striatal slices obtained from mice that were 4 weeks old, the AUC was the most important feature for determining whether a recording was made from the DLS or DMS with a frequency of 0.809. At 4 weeks of mouse age, the max[dF], ROI number, and decay dF were the prominent second-most important features with frequencies of 0.365, 0.284, and 0.167, respectively. Conversely, min[dF], Var[dF], and the two paroxysmal features were the least important features for distinguishing DLS from DMS at 4 weeks. At 8.5 weeks, the ROI number (frequency of 0.873) and decay dF (frequency of 0.857) were the most and second-most important features for distinguishing striatal brain region, respectively. In contrast to the 4 week time point, the AUC was among the least important features to distinguish brain region at 8.5 weeks, while Var[dF] was again deemed a feature unimportant to distinguish brain region, consistent with our 4 week analysis. At 12 weeks, ROI number is the most important feature to distinguish DLS from DMS with the highest frequency (0.859) while the two paroxysmal features and min[dF] are the least important features in the RF determination of the brain region that had stimulation-induced dopamine release measured by nIRCat. In sum, max[dF] and ROI number— representative of the maximum amount of dopamine released and the number of dopamine release sites, respectively—were consistently among the most important features to distinguish DLS from DMS striatal brain regions. Conversely, features associated with the variability of the baseline nIRCat nanosensor fluorescence, such as Var[dF] and min[dF], were consistently unimportant in distinguishing brain regions, as expected.

A strength of inference and prediction via machine learning lies in evaluating a multidimensional dataset, where a single predictive feature might not exist. Machine learning approaches can also facilitate a blind analysis of a dataset to avoid evaluator bias. Our machine learning algorithm highlighted max[dF] and ROI number as features that are consistently important across timepoints for distinguishing DLS from DMS brain regions. To verify that these features enable discrimination of nIRCat images taken from DLS versus DMS, we proceeded with a methodological analysis of our datasets, considering max[dF] and ROI number. We plotted the distribution of the features to visualize the difference in recorded values between DMS and DLS at each time point (Figures 5 and S1). In Figure S2, a two-sample Kolmogorov−Smirnov (KS) test was performed to determine whether the calculated features significantly vary between the nIRCat recordings collected from the DLS and DMS at a 0.3 mA stimulation strength. Interestingly, the only feature that met the significance criterion was the AUC when the recordings were made at 4 weeks. This corroborates the utility of the ML analysis in distinguishing differences that would otherwise not be identified as significant with conventional, univariate statistical techniques.

CONCLUSIONS

The past few years have seen the development of various tools to image neuromodulators, and specifically dopamine modulatory dynamics, at the spatiotemporal scales of relevance for endogenous neurochemical signaling. As these tools emerge, the rich datasets they generate in the form of videos of dopamine signaling dynamics provide many features, some of which may be more helpful than others in distinguishing biological phenomena. It is therefore of interest to develop and assess tools that quantify the release, volume transmission, and reuptake of neuromodulators, such as dopamine, where the observed spatial and temporal dynamics are dependent on dopamine receptor activation, dopamine transporter activity, neuronal activity, and neuronal tissue microstructure. It is also important to develop computational analyses to reduce bias, particularly those that analyze datasets manually.

In this manuscript, with features computed via dopamine nIRCat recordings, we are able to distinguish between striatal subregions and stimulation strengths in adult mice using a SVM and a random forest classifier. The latter addresses the bias-variance trade-off by reducing variance and avoiding overfitting, while the former provides robust performance. Our results indicate that an accurate discernment of the stimulation strength in the DLS and DMS is not possible from very young mice (i.e., prepubescent or young adult); however, as mice age, the distinguishability increases in both brain regions. The prediction accuracy of our machine learning algorithms consistently increases as a function of animal age. Increased variability in the kinetics and features of dopamine release in young animals is noted, and likely to contribute to this reduced accuracy in distinguishability. Our findings suggest that by the time animals reach adulthood (i.e., 12 weeks), it is possible that dopamine release and reuptake features have stabilized, thus enabling more accurate distinguishability among the stimulation strengths. The results are important to the growing community of dopamine

https://doi.org/10.1021/acschemneuro.3c00001
ACS Chem. Neurosci. XXXX, XXX, XXX−XXX

imaging researchers in motivating more careful consideration of cross-age group comparisons of dopamine signaling features.

Overall, higher predictive capabilities were noted with the statistical or combined features suggesting that the entire-recording statistics rather than the transient or paroxysmal aspects of dopamine modulatory kinetics are biomarkers of the striatal region from which the signals originated. Feature analysis enabled us to determine that the statistical properties of recordings rather than their transient or paroxysmal properties are more important in determining the striatal region where the dopamine release originated. Additionally, it is interesting that, similar to the age-dependent increase in the capability to distinguish among stimulation strengths, the differentiability of a brain region increased with the age of the animals. The results indicate that the dopamine release and reuptake dynamics are rather variable early in animal development but equilibrate in adulthood. The nascent research of dopamine imaging typically considers the magnitude of the change in the dopamine signal. Our results show that a machine learning approach can exploit a group of features (i.e., in Table 1) to discern neurochemical properties across brain regions in a manner that individual feature analysis does not. The ML approach provides a user-removed means for identifying changes in a manner that may not be practical, reproducible, or accurate with classical waveform analysis. The features that we have computed from the waveforms have physical meaning (e.g., the paroxysmal/burstiness of a waveform) that provide biological insight into attributes that are driving an outcome. By making use of biologically derived features from the waveforms, rather than the complete waveforms, the approach also provides a dimensionality reduction. Information is extracted from entire waveforms via single-number summary statistics prior to the ML analysis outputting the prediction.

Future advancements to this study are possible on the computational front. It would be advantageous to use more sophisticated kernel functions that are matched to the properties of the waveforms. This would involve deriving and incorporating a priori information from dopamine signals and the experimental conditions. The incorporation of additional features also constitutes an extension, for instance features that account for the timing properties of the waveforms such as τ_{off}. Furthermore, more complex classification tasks or combining different neuronal activity data types could enhance the accuracy at making correct predictions with neurochemistry datasets. For instance, adding more features could enhance the translation of all traces further enhancing our classification ability. Similarly, merging datasets from both neurochemical efflux and neuronal activity could further enhance the predictive capabilities of our algorithm. Nonetheless, our current study demonstrates that machine learning approaches are able to differentiate DLS from DMS striatal subregions of the mouse brain, in a manner unachievable with statistical analysis of the data alone. These findings suggest machine learning approaches to studying neurochemical dynamics could help differentiate between cohorts when classical statistical analyses find no differences with single-feature comparisons. For instance, recent study has shown that dopamine dynamics in late-stage Huntington's disease show a blunted ability to release dopamine at the single synapse level, and suggest that the dysregulation is driven by D2-autoreceptor regulation of dopamine release through Kv1.2 channels in late-stage Huntington's disease.[9] However, these findings were only shown to be statistically significant for late-stage Huntington's disease, despite trends at earlier timepoints that suggested dopamine signaling deficits present earlier in disease. Machine learning could help confirm the absence or presence of differences in such disease cohorts, potentially enabling the pinpointing of earlier onsets of variabilities in neurochemical signaling and what features of signaling drive the differences.

Herein, we have developed our machine learning algorithms and demonstrated their capabilities in differentiating datasets in a manner unachievable with statistical analysis of single features. However, the methods evoked in this study are not specific to dopamine signaling nor nIRCat-acquired data, rather they could be extrapolated to other time series data, such as additional neuromodulator probes emerging in the neuroimaging toolkit,[2−4] or imaging datasets of neuron activity, such as GCaMP-based probes. Expansion of this study can apply the same workflow to identify previously unnoticed trends. Moreover, future study may identify and introduce new features that raise the capability of a classifier. An exciting future avenue is to consider whether the above-mentioned neurochemical or neural activity datasets can collectively improve the precision of machine learning algorithms when trained on these different neuronal signals. It would be interesting to investigate whether the same features we identified in dopamine modulatory traces (i.e., peak dF/F and ROI number) are the most predictive for other neurotransmitters that exhibit different signaling dynamics in various brain regions. It is conceivable that separate machines must be trained to make predictions when considering different neurotransmitters, or that independent datasets would collectively enhance the performance of a machine despite inputs from different biological pathways. Beyond this study, many datasets exist in the literature and could readily benefit from machine learning and feature mining approaches. This includes analyses of neuronal activity and neurochemical signaling data from the growing number of neurotransmitter, neuromodulator, and neuropeptide optical probes.[2,4,15−19] Machine learning-based analysis of neurochemical imaging datasets could provide a user-independent approach to analyzing neurochemical imaging features and implementing those analyses to advance neurobiology research.

METHODS

nIRCat Sensor Production. The nIRCat nanosensor is produced by combining 100 μL of a 2 mg/mL solution of HiPCO raw single-walled carbon nanotubes (SWNT) suspended in molecular biology grade water, 100 μL of a 1× phosphate buffered saline (PBS) solution, and 100 μL of a 1 mM $(GT)_6$ ssDNA solution. The combined solution is probe tip sonicated for 10 min, then centrifuged at 16,000g for 30 min. The supernatant is then filtered through a 160k Da spin filter for 5 min at 8000g. The retentate is then resuspended in water and centrifuged for 5 min at 1000g. The resulting solution is a fully prepared nIRCat sensor. The sensor concentration is then calculated by using absorbance measured at 632 nm. Dopamine response is confirmed by measuring the fluorescence response of 2 mg/mL solutions of the sensor before and after addition of dopamine.[2,9−11]

Acute Brain Slice Generation and Sensor Labeling. All procedures involving animals were approved by the University of California, Berkeley Animal Care and Use Committee. Both male and female B6CBAF1/J mice (https://www.jax.org/strain/100011), were used for experiments. Mice were group-housed after weaning on postnatal day 21 (P21) with nesting material on a 12:12 light cycle. Acute brain slices were produced from three age groups: 4 weeks (P32−P35), 8.5 weeks (P64−P66), and 12 weeks (P87−P92). To generate acute brain slices, mice were anesthetized via intraperitoneal injection of a ketamine/xylazine cocktail. Mice were perfused transcardially using chilled, ascorbic acid-free cutting buffer (119 mM NaCl, 26.2 mM

https://doi.org/10.1021/acschemneuro.3c00001
ACS Chem. Neurosci. XXXX, XXX, XXX−XXX

$NaHCO_3$, 2.5 mM KCl, 1 mM NaH_2PO_4, 3.5 mM $MgCl_2$, 10 mM glucose, and 0 mM $CaCl_2$). The brain was extracted and mounted on a vibratome cutting stage (Leica VT1200 S) to produce 300 μm coronal slices containing the dorsal striatum. The slices were left in ACSF (119 mM NaCl, 26.2 mM $NaHCO_3$, 2.5 mM KCl, 1 mM NaH_2PO_4, 1.3 mM $MgCl_2$, 10 mM glucose, and 2 mM $CaCl_2$) to rest at 37 °C for 30 min followed by 30 min at room temperature. The slices were labeled with nanosensor by transferring the slices to a small volume incubation chamber containing oxygen-saturated ACSF and adding nIRCat nanosensor for a final concentration of 2 mg/L. The slices were subsequently rinsed in ACSF by transferring them through three wells of a 24-well plate and left to rest in ACSF for 15 min. The labeled slices were then transferred to the microscope recording chamber and allowed to equilibrate for 10 min before imaging. All imaging experiments were performed at 32 °C.

Stimulation and Image Collection. Following incubation with nIRCats, the slices were placed underneath a near-Infrared optical microscope.[2] Specific brain regions were identified using a 4× objective (Olympus XLFluor 4×/340). A bipolar stimulation electrode was placed 200 μm away from the region to be imaged. Using a 60× objective, 600 images were collected at a frame rate of 8.33 Hz, with a 100 ms stimulation occurring at the 200th frame. This process was repeated until the desired amount of replicates was achieved. During this process, the slices were kept viable by flowing an oxygenated ACSF solution held at 34 °C over the slices at a rate of 2 mL/min.

Image Processing. Image stacks were imported into MATLAB and were segregated into a grid consisting of 25 by 25 pixels (or roughly 7 by 7 microns), as prior study has established that the average dopamine release site volume transmission radius is 2 μm^2 and that 2 μm is an optimal grid size for nIRCat-based dopamine imaging analysis.[9] Each box within the grid was considered an ROI. A moving average was used to calculate the baseline of each ROI and subtracted from the original trace. The resulting trace left for the ROI was a time series of change in fluorescence. Between frames 200 and 300, the algorithm looked for an event that was 3 standard deviations above the average noise previously calculated for this ROI. If an event was found, this ROI was marked significant. If no event was detected, this ROI was deemed inactive and no more calculations are completed on this ROI. For each significant ROI, two exponentials were fit to the trace to determine the time constant of turn on and turn off. The algorithm also finds values, such as the maximum change in fluorescence and the area under the curve.[2]

Machine Learning Classification Methods. The SVM and RF algorithms were trained on the features in Table 1 to differentiate among the stimulation strength or the location of dopamine release, as described above. The SVM used a linear kernel with a binary classifier and was implemented in R via the packages e1071 and kernlab.[5] A linear kernel was used for simplicity and also the lack of a priori knowledge of the relationships between the features and the dynamics, as well as the source of dopamine release. The RF was implemented via the randomForest function and package in R.[6] The number of variables used for each split in the tree was specified as $\sqrt{p}$ with $p = 10$ or $p = 8$ for the scenarios of using the combined or statistical features, respectively. In all cases, the number of trees used, was 1000. However, we did not consider RF with the paroxysmal features, as there were too few variables (i.e., $p = 2$) to consider this as worthwhile analysis. The evaluation of the predictive capability via the classifier AR entailed a leave-one-out analysis with Monte-Carlo (MC) sampling of the brain slices. The MC analysis entailed the data being repeatedly divided into a training and test set with the test data consisting of a single observation, while the remaining data was evenly partitioned into two groups and used to train the machine. The classification decisions that consisted of distinguishing between possible stimulation strength or brain regions were binary. For each scenario, the accuracy rates for the two possibilities were presented in the figures. The third consideration deemed the "aggregate" consisted of averaging the two accuracy rates to provide a holistic account. Our consideration of feature importance used the node purity metric in the RF technique. The metric was used to evaluate which of the stimulated dopamine features were the most important in the classifiers' decisions of the brain region.

■ ASSOCIATED CONTENT

Data Availability Statement

The custom-built MATLAB program used to process the Raw Image stack files are publicly available at https://github.com/jtdbod/Nanosensor-Imaging-App. The rest of the data and code are available upon request.

Supporting Information

The Supporting Information is available free of charge at https://pubs.acs.org/doi/10.1021/acschemneuro.3c00001.

Swarm plots of max[dF] and ROI number across age groups and DLS versus DMS brain regions; univariate statistical analysis of features from the DLS and DMS for 0.3 mA stimulation strength across all three age groups (PDF)

■ AUTHOR INFORMATION

Corresponding Author

Markita P. Landry − *Department of Chemical and Biomolecular Engineering, University of California,, Berkeley, California 94720, United States; Innovative Genomics Institute, Berkeley, California 94720, United States; California Institute for Quantitative Biosciences, University of California, Berkeley, California 94720, United States; Chan Zuckerberg Biohub, San Francisco, California 94063, United States;* orcid.org/0000-0002-5832-8522; Email: landry@berkeley.edu

Authors

Siamak K. Sorooshyari − *Department of Integrative Biology, University of California, Berkeley, California 94720, United States;* orcid.org/0000-0002-1172-6291

Nicholas Ouassil − *Department of Chemical and Biomolecular Engineering, University of California,, Berkeley, California 94720, United States*

Sarah J. Yang − *Department of Chemical and Biomolecular Engineering, University of California,, Berkeley, California 94720, United States;* orcid.org/0000-0001-5950-3006

Complete contact information is available at: https://pubs.acs.org/10.1021/acschemneuro.3c00001

Author Contributions

N.O., S.Y., and M.L. designed the experiments. N.O. and S.Y. performed the experiments and data collection. S.S. conducted the computational and machine learning analysis. S.S., N.O. and S.Y. wrote the manuscript with feedback from M.L.

Notes

The authors declare no competing financial interest.

■ ACKNOWLEDGMENTS

We acknowledge the support of a Burroughs Wellcome Fund Career Award at the Scientific Interface (CASI) (MPL), a Dreyfus foundation award (MPL), the Philomathia foundation (MPL), an NIH MIRA award R35GM128922 (MPL), an NIH R21 NIDA award 1R03DA052810 (MPL), an NSF CAREER award 2046159 (MPL), an NSF CBET award 1733575 (to MPL), a CZI imaging award (MPL), a Sloan Foundation Award (MPL), a USDA BBT EAGER award (MPL), a Moore Foundation Award (MPL), and a DOE office of Science grant DE-SC0020366 (MPL). MPL is a Chan Zuckerberg Biohub investigator, a Hellen Wills Neuroscience Institute Investigator, and an IGI Investigator.

REFERENCES

(1) Bulumulla, C.; Krasley, A.; et al. Visualizing synaptic dopamine efflux with a 2D composite nanofilm. *eLife* **2022**, *11*, No. e78773.
(2) Beyene, A.; Delevich, K.; et al. Imaging striatal dopamine release using a nongenetically encoded near infrared fluorescent catecholamine nanosensor. *Sci. Adv.* **2019**, *5*, No. eaaw3108.
(3) Sun, F.; Zeng, J.; et al. A genetically encoded fluorescent sensor enables rapid and specific detection of dopamine in flies, fish, and mice. *Cell* **2018**, *174*, 481−496.e19.
(4) Patriarchi, T.; Cho, J.; et al. Ultrafast neuronal imaging of dopamine dynamics with designed genetically encoded sensors. *Science* **2018**, *360*, No. eaat4422.
(5) Karatzoglou, A.; Smola, A.; Hornik, K. *kernlab: Kernel-Based Machine Learning Lab. R package version 0.9-30*, 2022. https://CRAN.R-project.org/package=kernlab.
(6) Liaw, A.; Wiener, M. *Classification and Regression by randomForest, R package version 4.7-1*, https://cran.r-project.org/web/packages/randomForest/index.html, 2002.
(7) Calipari, E.; Huggins, K.; Mathews, T.; Jones, S. Conserved dorsal-ventral gradient of dopamine release and uptake rate in mice, rats and rhesus macaques. *Neurochem. Int.* **2012**, *61*, 986−991.
(8) Kaplan, S.; Limbocker, R.; Levant, B.; Johnson, M. Regional differences in dopamine release in the R6/2 mouse caudate putamen. *Electroanalysis* **2018**, *30*, 1066−1072.
(9) Yang, S.; Del Bonis-O'Donnell, J. et al., Synaptic scale dopamine disruption in Huntington's Disease model mice imaged with near infrared catecholamine nanosensors. *bioRxiv* , DOI: 10.1101/2022.09.19.508617.
(10) Yang, S.; Del Bonis-O'Donnell, J.; et al. Near-infrared catecholamine nanosensors for high spatiotemporal dopamine imaging. *Nat. Protoc.* **2021**, *16*, 3026−3048.
(11) Yang, D.; Yang, S.; del Bonis-O'Donnell, J. T.; Pinals, R. L.; Landry, M. P. Mitigation of carbon nanotube neurosensor induced transcriptomic and morphological changes in mouse microglia with surface passivation. *ACS Nano* **2020**, *14*, 13794−13805.
(12) Wickens, J.; Budd, C.; Hyland, B.; Arbuthnott, G. Striatal contributions to reward and decision making: making sense of regional variations in a reiterated processing matrix. *Ann. N. Y. Acad. Sci.* **2007**, *104*, 192−212.
(13) Arbuthnott, G.; Wickens, J. Space, time and dopamine. *Trends Neurosci.* **2007**, *30*, 62−69.
(14) Lovinger, D.; Mathur, B. Endocannabinoid signaling in the striatum. *Handbook of Behavioral Neuroscience*; Elsevier, 2010; pp 167−186.
(15) Kelich, P.; Jeong, S.; et al. Machine learning enables discovery of DNA-carbon nanotube sensors for serotonin. *bioRxiv* **2021**, DOI: 10.1101/2021.08.20.457145.
(16) Jeong, S.; Yang, D.; et al. High throughput evolution of near infrared serotonin nanosensors. *Sci. Adv.* **2019**, *5*, No. eaay3771.
(17) Dorlhiac, G.; Streets, A.; Landry, M. Leveraging Isotopologues as a general strategy to image neurotransmitters with vibrational microscopy. *arXiv:2205.05798*.
(18) Navarro, N.; Jeong, S.; et al. Near infrared nanosensors enable optical imaging of oxytocin with selectivity over vasopressin in acute mouse brain slices. *bioRxiv* **2022**, DOI: 10.1101/2022.10.05.511026.
(19) Qian, T.; Wang, H.; et al. A genetically encoded sensor measures temporal oxytocin release from different neuronal compartments. *Nat. Biotechnol.* **2023**, 1−14.
(20) Schmidt, K.; McElligott, Z. Dissecting the catecholamines: how new approaches will facilitate the distinction between noradrenergic and dopaminergic systems. *ACS Chem. Neurosci.* **2019**, *10*, 1872−1874.
(21) Behboodi-Sadabad, F.; Li, S.; et al. High-throughput screening of multifunctional nanocoatings based on combinations of polyphenols and catecholamines. *Mater. Today Bio* **2021**, *10*, No. 100108.
(22) Hassani-Marand, M.; Fahimi-Kashani, N.; Hormozi-Nezhad, M. Machine-learning assisted multiplex detection of catecholamine neurotransmitters with a colorimetric sensor array. *Anal. Methods* **2023**, *15*, 1123−1134.
(23) Jia, W.; Hu, C.; et al. Identification of single-molecule catecholamine enantiomers using a programmable nanopore. *ACS Nano* **2022**, *16*, 6615−6624.
(24) Beyene, A.; Alizadehmojarad, A.; Dorlhiac, G.; Goh, N.; Streets, A. M.; Král, P.; Vuković, L.; Landry, M. P. Ultralarge modulation of fluorescence by neuromodulators in carbon nanotubes functionalized with self-assembled oligonucleotide rings. *Nano Lett.* **2018**, *18*, 6995−7003.
(25) Elizarova, S.; Chouaib, A.; Shaib, A.; Hill, B.; Mann, F.; Brose, N.; Kruss, S.; Daniel, J. A. A fluorescent nanosensor paint detects dopamine release at axonal varicosities with high spatiotemporal resolution. *Proc. Natl. Acad. Sci. U. S. A.* **2022**, *119*, No. e2202842119.
(26) Koda, T.; Ago, Y.; Cong, Y.; Kita, Y.; Takuma, K.; Matsuda, T. Effects of acute and chronic administration of atomoxetine and methylphenidate on extracellular levels of noradrenaline, dopamine and serotonin in the prefrontal cortex and striatum of mice. *J. Neurochem.* **2010**, *114*, 259−270.

https://doi.org/10.1021/acschemneuro.3c00001
ACS Chem. Neurosci. XXXX, XXX, XXX−XXX